BBA - Molecular Basis of Disease 1865 (2019) 1351–1360

Contents lists available at ScienceDirect

BBA - Molecular Basis of Disease

journal homepage: www.elsevier.com/locate/bbadis

Impact of apolipoprotein A1- or lecithin:cholesterol acyltransferase-deficiency on white adipose tissue metabolic activity and glucose homeostasis in mice

Eva Xepapadaki[a], Giuseppe Maulucci[b,c], Caterina Constantinou[a], Eleni A. Karavia[a], Evangelia Zvintzou[a], Bareket Daniel[d], Shlomo Sasson[d], Kyriakos E. Kypreos[a,*]

[a] University of Patras, School of Medicine, Department of Pharmacology, Rio, Achaias, TK. 26500, Greece
[b] Fondazione Policlinico Universitario A.Gemelli IRCSS, Rome, Italy
[c] Istituto di Fisica, Università Cattolica del Sacro Cuore Roma, Italy
[d] Department of Pharmacology, Institute for Drug Research, Faculty of Medicine, The Hebrew University, Jerusalem, Israel

ARTICLE INFO

Keywords:
High density lipoprotein
Apolipoprotein A1
Lecithin-cholesterol acyltransferase
Diabetes
Pancreatic β-cells
Insulin
Skeletal muscle

ABSTRACT

High density lipoprotein (HDL) has attracted the attention of biomedical community due to its well-documented role in atheroprotection. HDL has also been recently implicated in the regulation of islets of Langerhans secretory function and in the etiology of peripheral insulin sensitivity. Indeed, data from numerous studies strongly indicate that the functions of pancreatic β-cells, skeletal muscles and adipose tissue could benefit from improved HDL functionality. To better understand how changes in HDL structure may affect diet-induced obesity and type 2 diabetes we aimed at investigating the impact of Apoa1 or Lcat deficiency, two key proteins of peripheral HDL metabolic pathway, on these pathological conditions in mouse models. We report that universal deletion of *apoa1* or *lcat* expression in mice fed western-type diet results in increased sensitivity to body-weight gain compared to control C57BL/6 group. These changes in mouse genome correlate with discrete effects on white adipose tissue (WAT) metabolic activation and plasma glucose homeostasis. Apoa1-deficiency results in reduced WAT mitochondrial non-shivering thermogenesis. Lcat-deficiency causes a concerted reduction in both WAT oxidative phosphorylation and non-shivering thermogenesis, rendering *lcat*$^{-/-}$ mice the most sensitive to weight gain out of the three strains tested, followed by *apoa1*$^{-/-}$ mice. Nevertheless, only *apoa1*$^{-/-}$ mice show disturbed plasma glucose homeostasis due to dysfunctional glucose-stimulated insulin secretion in pancreatic β-islets and insulin resistant skeletal muscles. Our analyses show that both *apoa1*$^{-/-}$ and *lcat*$^{-/-}$ mice fed high-fat diet have no measurable Apoa1 levels in their plasma, suggesting no direct involvement of Apoa1 in the observed phenotypic differences among groups.

1. Introduction

High density lipoprotein (HDL) is a macromolecular assembly of proteins and lipids circulating in blood. In recent decades it has attracted the attention of the biomedical community mainly due to the inverse relationship between blood HDL-cholesterol (HDL-C) levels

Abbreviations: ABCA1, ATP-binding cassette A1; ABCG1, ATP-binding cassette G1; APOA1, human apolipoprotein A-I; Apoa1, murine apolipoprotein A-I; *apoa1*, murine gene of Apoa1; *apoa1*$^{-/-}$, Apoa1 deficient mouse; Apoa2, murine apolipoprotein A-II; Apoc1, murine apolipoprotein C-I; Apoc2, murine apolipoprotein C-II; APOC3, human apolipoprotein C-III; Apoc3, murine apolipoprotein C-III; APOE, human apolipoprotein E; Apoe, murine apolipoprotein E; ATP, adenosine triphosphate; AUC, area under the curve; BAT, brown adipose tissue; BRITE, brown into white; CETP, cholesteryl-ester transfer protein; CHD, coronary heart disease; Cox4, murine cytochrome *c* oxidase subunit 4; Cytc, murine cytochrome *c*; DMSO, dimethyl sulfoxide; GP, generalized polarization; GSIS, glucose stimulated insulin secretion; GTT, glucose tolerance test; HDL, high-density lipoprotein; HDL-C, HDL-cholesterol; HOMA, homeostasis model assessment; IDL, intermediate-density lipoproteins; IST, insulin sensitivity test; ISUG, Insulin stimulated [^{3}H]-2-deoxy-D-glucose uptake; KCl, potassium chloride; LCAT, human lecithin:cholesterol acyl transferase; Lcat, murine lecithin:cholesterol acyl transferase; *lcat*, murine gene of Lcat; *lcat*$^{-/-}$, Lcat deficient mouse; LDL, low-density lipoproteins; PLTP, phospholipid transfer protein; PTT, pyruvate tolerance test; S.D, standard deviation; S.E.M, standard error of the mean; T2DM, type 2 diabetes mellitus; UCF, ultracentrifugation; Ucp1, murine uncoupling protein 1; VLDL, very low-density lipoproteins; WAT, white adipose tissue

* Corresponding author at: University of Patras Medical School, Department of Medicine, Pharmacology Laboratory, Panepistimioupolis, Rio, TK 26500, Greece.
E-mail address: kkypreos@med.upatras.gr (K.E. Kypreos).
URL: http://www.kyriakoskypreos.com (K.E. Kypreos).

https://doi.org/10.1016/j.bbadis.2019.02.003
Received 19 November 2018; Received in revised form 4 February 2019; Accepted 6 February 2019
Available online 10 February 2019
0925-4439/

with the risk of developing atherosclerosis and coronary heart disease (CHD) [1–7]. However, the failure of a number of HDL-C raising drugs to reduce CHD morbidity and mortality [4,5] led to the conclusion that simply increasing plasma HDL-C levels only may not be an effective strategy for the prevention and treatment of CHD [4,7]. Moreover, it reinforced the principle that HDL particle functionality may be more important in atheroprotection than HDL-C levels alone [4,7].

HDL particles may be discoidal or spherical with varying diameters [8]. Their biogenesis involves lipid transporters ATP-binding cassette A1 and G1 (ABCA1 and ABCG1, respectively) which are responsible for cholesterol efflux, and the plasma enzyme Lecithin:Cholesterol Acyl Transferase (LCAT), which catalyzes the esterification of free cholesterol and converts HDL from discoidal to spherical particles. In addition, cholesteryl-ester transfer protein (CETP) and phospholipid transfer protein (PLTP) further process HDL in plasma, resulting in spherical particles of different diameters [9–13]. Studies in mouse models showed that in addition to apolipoprotein A1 (APOA1) other apolipoproteins, such as APOE [14] and APOC3 [15] may also promote de novo biogenesis of HDL, independently of pre-existing classical APOA1-containing HDL [4]. APOE- and APOC3-containing HDL particles appear structurally and functionally distinct from APOA1-containing HDL and from each other [16,17]. Notably, the apolipoprotein composition of HDL is a decisive factor for its lipid cargo and overall functionality [16–19]. In agreement with data from animal studies, studies in humans indicate that variations in apolipoprotein content of HDL set the basis for its functional heterogeneity among individuals [20], and that differences in lipid composition may result in HDL of either discoidal or spherical shapes [4,7]. Specifically, reduced levels of APOA1 and concomitant elevated content of APOC3 and APOE in HDL correlate with less functional HDL [18,19].

Adipose tissue consists of white adipose tissue (WAT) and brown adipose tissue (BAT): the former is mainly responsible for lipid storage, and the latter for energy production (heat and ATP). Under certain circumstances WAT may be activated metabolically and turn into BRITE (BRown Into whiTE) adipose tissue that can produce heat via non-shivering thermogenesis [21]. The latter phenomenon results from an elevated mitochondrial metabolic activity, mainly of uncoupling protein 1 (Ucp1) function, which mediates the metabolic conversion of free fatty acids to heat, thus contributing to the lean phenotype [22,23]. However, induction of WAT mitochondrial oxidative phosphorylation for ATP production, independently of Ucp1 increase, may also contribute to the lean phenotype [24]. Metabolic activation of WAT into BRITE is considered a promising strategy for treatment of morbid obesity and numerous experimental drugs have been designed towards this goal, though to this date the molecular targets for such interventions remain vague. It is generally agreed that dysfunctional adipose organ predisposes to type 2 diabetes mellitus (T2DM) and other pathological components of the metabolic syndrome [25].

T2DM is a major global health problem, affecting over 300 million people worldwide [26]. It develops because of reduced glucose tolerance, initially manifested as peripheral resistance, and consequently impaired insulin production and secretion by pancreatic β-cells. Recently, considerable attention has been put on the role of HDL in the regulation of β-cell secretory function and peripheral insulin sensitivity. Indeed, data from numerous studies strongly support the hypothesis that pancreatic β-cells, as well as skeletal muscles and adipose tissues could benefit from improved HDL functionality [27]. Yet, although many studies explored the correlation between HDL-C levels and the risk of developing T2DM [27–29], the effects of HDL structure on the disease remain poorly investigated.

To understand how structural changes in HDL may affect morbid obesity and diabetes, we compared in the present study the effects of Apoa1- and Lcat-deficiency on diet-induced weight gain, WAT mitochondrial metabolism and plasma glucose homeostasis in mice.

2. Material and methods

2.1. Animals

Female C57BL/6, and *apoa1*$^{-/-}$ mice 10–12 weeks old were purchased from Jackson Labs (Bar Harbor, Maine, USA). The *lcat*$^{-/-}$ mice were a generous gift of Dr. Silvia Santamarina-Fojo [30]. Both *apoa1*$^{-/-}$ and *lcat*$^{-/-}$ mouse models were back-crossed on the C57BL/6 background for at least 10 generations. Mice in each group were caged individually and were allowed unrestricted access to food and water under a 12 h light/dark cycle. All animals employed in the study were fed the standard western type diet (Mucedola SRL. Milano, Italy) that contains 4.5 kcal/g (17.3% protein, 48.5% carbohydrate, 21.2% fat, 0.2% cholesterol) for the indicated periods. At the end of each experiment, mice were euthanatized, and plasma and tissue samples were collected. All animal studies were conducted according to the EU guidelines of the *Protocol for the Protection and Welfare of Animals*. The estimated sample size was determined based on the desired power of statistical analysis, using an online statistical tool (http://www.stat.ubc.ca/~rollin/stats/ssize/n2.html). The work was approved by the appropriate committee of the Laboratory Animal Center of The University of Patras Medical School and the Veterinary Authority of the Prefecture of Western Greece.

2.2. Determination of body weight and plasma lipids

Mice were briefly anesthetized using isofluorane and weighted on a Mettler® precision microscale. Plasma total cholesterol and triglyceride levels were assessed spectrophotometrically following a 16 h fasting period, as described previously [31]. The DiaSys Cholesterol FS kit (cat# 113009910021, Diagnostic Systems GmbH, Holzheim, Germany) and the DiaSys Triglycerides FS kit (cat# 157109910021, Diagnostic Systems GmbH, Holzheim, Germany) respectively, were employed according to the manufacturers' instructions.

2.3. Intraperitoneal glucose tolerance (GTT), insulin sensitivity (IST) and pyruvate tolerance tests (PTT)

Prior analysis mice were fasted for 16 h. GTT, IST and PTT were performed as described previously [32] and blood glucose determination was performed at the indicated time–points of each test. Plasma glucose was determined by DiaSys Glucose FS kit (cat# 125009910021, Diagnostic Systems GmbH, Holzheim, Germany).

2.4. Determination of post-prandial plasma triglyceride kinetics and tissue distribution following oral administration of olive oil

A modification of the method of Augustus et al. was used [33] as described previously [34]. Specifically, groups of *apoa1*$^{-/-}$, *lcat*$^{-/-}$, and control C57BL/6 mice were gavage fed 200 μl of extra virgin olive oil, containing 59.2 KBq [^{3}H]-triolein with specific activity 2.22 TBq/mmol (American Radiolabeled Chemicals, Inc., Triolein [9,10-^{3}H (N)] cat# ART0199) and 5.92 KBq [^{14}C]-cholesterol with specific activity 1.85 GBq/mmol (American Radiolabeled Chemicals, [4-^{14}C]-Cholesterol cat# ARC0857). [^{3}H]-triolein served a tracer for plasma triglyceride clearance while [^{14}C]-cholesterol served as a tracer for plasma cholesterol and lipoprotein remnant clearance. At 240 min, mice were sacrificed, perfused with sterile cold saline for 3 min, liver, soleus muscle, BAT, visceral WAT and islets of Langerhans were collected and their [^{3}H] and [^{14}C] content was determined by liquid scintillation in a Beckman β-counter model LS6500 (Beckman Coulter, Brea CA, USA). Values were expressed in cpm of each isotope/g tissue ± standard error of the mean (S.E.M).

2.5. Fractionation of plasma lipoproteins by density gradient ultracentrifugation

Isolated plasma samples from ten mice per group were pooled and 0.4 ml of pools were fractionated by density gradient ultracentrifugation (UCF) over a 4 ml KBr (Sigma-Aldrich, St. Louis, MO, USA) density gradient in a Beckmann-Coulter Ultracentrifuge (Indianapolis, IN, USA) using an SW60 rotor, as described previously [17].

2.6. Isolation of mitochondria

Mitochondria from BAT and WAT were isolated as described previously [35]. The protein concentration of each mitochondrial sample was determined by the Lowry assay using the DCTM Protein Assay Kit (cat# 500-0116, Bio-Rad, USA).

2.7. Western blot analysis

For the semiquantitative measurement of Apoa1, Apoa2, Apoe, Apoc1, Apoc2 and Apoc3 in lipoprotein fractions, Western blot analysis was performed as described previously [17,34,35]. For the detection of Apoa1, Apoe and Apoc3 rabbit anti-Apoa1 (cat# AP23390PU-N, Acris), anti-Apoe (cat# K23100R, Meridian Life Science) and anti-Apoc3 (cat# ab55984, Abcam and cat# PAB5869, Abnova) were used respectively as primary and a goat anti-rabbit antibody (cat#7074, Cell Signaling) as secondary. Goat anti-Apoa2 (cat# K34001G), anti–Apoc1 (cat# K74110G) and anti-Apoc2 (cat# K59600R) antibodies from Meridian Life Science, USA, were used respectively as primary, and a rabbit anti-goat antibody (cat# sc-2768, Santa-Cruz) as secondary. Western blotting for Cytc, Ucp1, and Cox4 was performed using IgG primary rabbit anti-mouse antibodies (cat# 4272, Cell Signaling; Danvers, MA, USA; cat# GTX10983, Acris, Herford, Germany; cat# 4844, Cell Signaling, Danvers, MA, respectively). SDS-PAGE of pure mitochondrial extracts was performed using 6 μg protein/sample for BAT and 10 μg protein/sample for WAT. Semiquantitative determination of the relative protein amounts was performed by Image J free software and Cytc and Ucp1 levels were normalized to Cox4 levels.

2.8. Insulin stimulated [^{3}H]-2-deoxy-D-glucose uptake assay (ISGU) in isolated soleus muscles

Soleus muscle glucose uptake, in the presence or absence of insulin stimulation, was determined as described previously [36]. Briefly, mice were fasted for 16 h and then sacrificed and both soleus muscles from each animal were dissected and incubated in a buffer solution containing 0.37 MBq/ml [^{3}H]-2-deoxy-D-glucose (American Radiolabelled Chemicals, St. Louis, MO, USA, cat#ART0103A, with specific activity 2.22 TBq/mmol) in the presence (+insulin) or absence (−insulin) of 500 nM actrapid insulin U-100 (Novo Nordisk, Denmark).

2.9. HOMA index calculation

As an additional measure of insulin sensitivity, the homeostasis model assessment (HOMA) index was calculated from the fasting plasma glucose and insulin levels as follows: HOMA = (fasting glucose concentration [md/dl] x fasting insulin concentration [mU/l])/405 [37,38]. Plasma glucose was determined by DiaSys Glucose FS kit (cat# 125009910021, Diagnostic Systems GmbH, Holzheim, Germany) while plasma insulin levels were measured by ELISA (Merck Millipore, Billerica, MA, USA cat# EZRMI-13).

2.10. Islets of Langerhans isolation and glucose stimulated insulin secretion assay

Islets of Langerhans were isolated from mice of each group, following collagenase digestion of pancreases and ex vivo glucose stimulated insulin secretion (GSIS) assay was performed, as described previously [39]. Briefly, isolated islets were successively incubated in Krebs-Ringer bicarbonate HEPES-BSA buffer containing different concentrations of glucose (3.3 mM and 16.7 mM) and finally in lysis buffer. All incubations were performed at 37 °C for 1 h. Islets from C57BL/6 or *apoa1*$^{-/-}$ mice were also incubated for 1 h in Krebs-Ringer bicarbonate HEPES-BSA buffer containing 3.3 mM glucose in the presence or absence of 40 mM KCl, in order to exogenously stimulate the plasma membrane depolarization and subsequent insulin secretion. Supernatants of each incubation were collected, and insulin levels were measured by ELISA (Merck Millipore, Billerica, MA, USA cat# EZRMI-13).

2.11. Two-photon microscopy analysis of cell membrane fluidity in isolated islets of Langerhans

To determine the effects that structural changes of HDL exert on cell membrane fluidity of freshly isolated islets of Langerhans, two-photon microscopy analysis using Laurdan stain was performed. Briefly, islets were incubated in 1 mM Laurdan (Molecular Probes, Inc., Eugene, OR, USA) in dimethyl sulfoxide (DMSO; Sigma, St. Louis, MO) in a 5% CO_2 incubator for 30 min in the dark. Afterwards, the slide was placed on the inverted confocal microscope (DMIRE2, Leica Microsystems, Germany) and Laurdan intensity images were obtained using a 60× objective (NA 1.4) under excitation at 800 nm with a mode-locked Titanium-Sapphire laser (Chameleon, Coherent, Santa Clara, CA). Internal photon multiplier tubes collected images in an eight-bit, unsigned images at a 400 Hz scan speed. Laurdan intensity images were recorded simultaneously with emission in the range of 400–460 nm and 470–530 nm and imaging was performed at room temperature. For each specimen, 4–6 field images were analyzed first with the software GPicture [40]. The program measures membrane fluidity in terms of ratio of emission intensities by using Generalized Polarization (GP) value [41]. GP value was calculated for each pixel using the two Laurdan intensity images [I(400–460) and I(470–530)]. The calibration factor G was obtained from the GP values of solutions of Laurdan in DMSO. GP images (as eight-bit unsigned images) were pseudocoloured in Image-J. GP histograms values were determined within multiple Regions of Interest (plasma membranes of single cells) for each sample, and their mean ± standard deviation (S.D) determined and utilized for further statistical analysis (two-tailed Student's *t*-test). Line profiles and analysis of acquired images were performed with Image J free software.

2.12. Statistical analysis

Data are reported as Mean ± S.E.M or Mean ± S.D. * indicates $P \leq 0.05$, ** indicates $P < 0.01$. n indicates the number of animals tested in each experiment. Data sets were tested using the Kolmogorov-Smirnov and the Shapiro-Wilk tests and were treated with parametric ($P > 0.1$) or non-parametric tests ($P < 0.1$) according to their deviation from normality. All statistical tests were performed using the GraphPad Prism 6.0 (GraphPad Software, Inc., La Jolla, CA, US).

3. Results

3.1. Effects of feeding high-fat diet on body weight gain, plasma lipid levels and lipoprotein and apolipoprotein distribution

To determine the effects of Apoa1- and Lcat-deficiency on body weight gain, *apoa1*$^{-/-}$ and *lcat*$^{-/-}$ mice were fed *ad libidum* western-type diet for 24 weeks: body weights (Fig. 1A) and plasma lipids (Fig. 1B, C) were determined at the beginning and at the end of the experiment. At the beginning all mice had similar body weight (16.88 ± 0.3 g for C57BL/6, 19.66 ± 0.33 g for *apoa1*$^{-/-}$ and 17 ± 0.57 g for *lcat*$^{-/-}$, all $P > 0.05$), which significantly increased during the course of the diet (Fig. 1A). Indeed, at week 24 the average

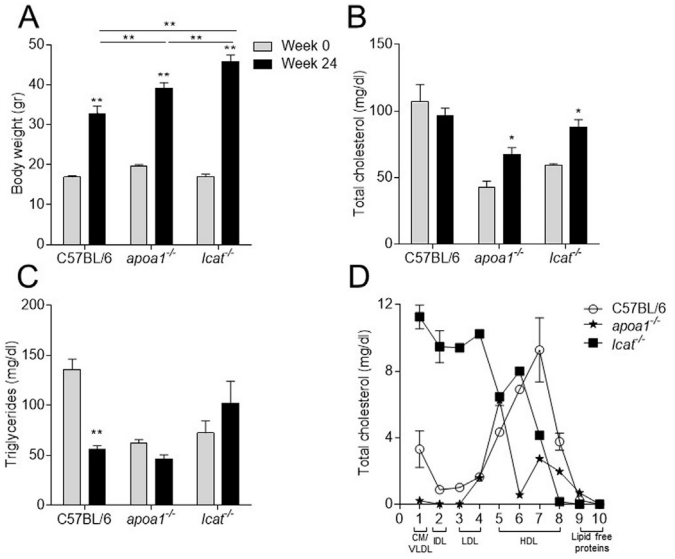

Fig. 1. Body weight, plasma triglyceride and cholesterol levels of C57BL/6, *apoa1*$^{-/-}$ and *lcat*$^{-/-}$ mice at the beginning of the experiment (week 0) or 24 weeks after feeding western-type diet (week 24). (A) Body weight, (B) plasma total cholesterol levels and (C) plasma triglyceride levels. (D) Total cholesterol levels of plasma lipoprotein fractions isolated by KBr density gradient ultracentrifugation (UCF) from plasma samples of C57BL/6, *apoa1*$^{-/-}$ and *lcat*$^{-/-}$ mice after 24 weeks of feeding western-type diet. Data were analyzed using Student's *t*-test and are presented as mean ± S.E.M (n = 4–9).

body weight of C57BL/6 mice reached 32.46 ± 1.89 g whereas *apoa1*$^{-/-}$ and *lcat*$^{-/-}$ mice were significantly heavier reaching 39.08 ± 1.42 g and 45.83 ± 1.62 g, respectively (both $P < 0.001$ compared to C57BL/6 group) (Fig. 1A).

Given that the lipoprotein system is responsible for the management of dietary lipids in circulation, we further investigated the effects of Apoa1 and Lcat deficiency on plasma lipoprotein and apolipoprotein profiles. Peripheral blood samples were isolated from *apoa1*$^{-/-}$, *lcat*$^{-/-}$ and C57BL/6 mice at the end of week 24 and plasma cholesterol and triglyceride levels were measured. Total plasma cholesterol levels were below 100 mg/dl for all mouse strains (95.6 ± 5.7 mg/dl, 67.2 ± 5.2 mg/dl and 87.9 ± 5.5 mg/dl for C57BL/6, *apoa1*$^{-/-}$ and *lcat*$^{-/-}$ mice, respectively) (Fig. 1B). Similarly, plasma triglyceride levels were below 150 mg/dl for all mouse strains (55.7 ± 4.0 mg/dl, 46.5 ± 4.1 mg/dl and 102.5 ± 21.5 mg/dl for C57BL/6, *apoa1*$^{-/-}$ and *lcat*$^{-/-}$ mice, respectively) (Fig. 1C). Then, lipoprotein fractions were purified by KBr density gradient UCF (Fig. 1D). Both *apoa1*$^{-/-}$ and *lcat*$^{-/-}$ mice on western type diet exhibited reduced HDL-C levels compared to their C57BL/6 counterparts, while *lcat*$^{-/-}$ mice displayed a notable shift of their plasma cholesterol towards VLDL, IDL and LDL fractions (Fig. 1D). As expected, control C57BL/6 mice had mainly HDL in their peripheral circulation.

Western blot analysis of apolipoproteins of the purified lipoprotein fractions revealed that HDL from all three mouse strains presented discrete apolipoprotein composition (Fig. 2): HDL from *apoa1*$^{-/-}$ mice contained mainly Apoe and Apoc2, low level of Apoa2 and trace amount of Apoc1. On the other hand, HDL from *lcat*$^{-/-}$ mice contained primarily Apoa2, Apoe, and trace amount of Apoc1. As expected, HDL from control C57BL/6 mice contained mainly Apoa1, Apoa2 and Apoc2, and a lower level of Apoe.

3.2. Post-prandial triglycerides and cholesterol tissue distribution

Next, we investigated whether the differences in plasma lipoprotein and apolipoprotein profiles were associated with changes in post-prandial triglyceride and cholesterol tissue accumulation, thus contributing to differences in body weight gain among groups (Fig. 3). A*poa1*$^{-/-}$, *lcat*$^{-/-}$ and C57BL/6 mice were gavage fed olive oil containing [^{3}H]-triolein and [^{14}C]-cholesterol and their liver, soleus muscle, BAT, visceral WAT and pancreatic islets were collected and their [^{3}H] and [^{14}C] content was determined, as described in Methods.

Measurement of the [^{3}H] radioactive tracer following gavage feeding, showed a significantly lower dietary triglyceride tissue deposition in WAT of *apoa1*$^{-/-}$ and *lcat*$^{-/-}$ mice even though they became more obese than the control C57BL/6 mice upon feeding western-type diet. Interestingly, there was also reduced [^{3}H]-tracer deposition in isolated pancreatic islets of Langerhans (Fig. 3A). No differences in [^{3}H] levels among groups were identified in liver, BAT and soleus muscle.

Measurement of [^{14}C] radioactive tracer, following the gavage showed no difference in WAT [^{14}C]-tracer levels among groups. Nevertheless, *apoa1*$^{-/-}$ mice accumulated higher amounts of [^{14}C]-tracer in BAT and soleus muscle, suggesting increased dietary cholesterol deposition in these tissues (Fig. 3B).

3.3. Effects of Apoa1 and Lcat deficiency on BAT and WAT mitochondrial metabolic activity

We then determined the effects of Apoa1- and Lcat-deficiency on visceral WAT and BAT metabolic activity. Groups of *apoa1*$^{-/-}$, *lcat*$^{-/-}$ and C57BL/6 mice were fed western-type diet for 24 weeks and then pure visceral WAT and BAT mitochondria were isolated and analyzed for Cytc, Ucp1 and Cox4 protein levels (Fig. 4). Comparable levels of Cytc were found in WAT mitochondria, of *apoa1*$^{-/-}$ and C57BL/6 mice, indicative of similar levels of oxidative phosphorylation in this tissue. Interestingly, *lcat*$^{-/-}$ mice exhibited significantly lower Cytc levels, suggesting that lack of functional Lcat has a selective negative impact on WAT mitochondrial oxidative phosphorylation. The significant level of Ucp1 in WAT mitochondria from C57BL/6 mice, were drastically reduced in *apoa1*$^{-/-}$ and *lcat*$^{-/-}$ mice, indicating attenuated substrate oxidation towards thermogenesis in WAT of these animals (Fig. 4A, C, E). Ucp1 levels in WAT mitochondria from *lcat*$^{-/-}$ mice were lower than in *apoa1*$^{-/-}$ mice ($P < 0.01$).

Similar analysis of purified BAT mitochondrial extracts revealed comparable levels of Cytc in all three mouse strains indicative of similar oxidative phosphorylation. When Ucp1 was measured in these mitochondrial extracts we observed a rather small increase in *apoa1*$^{-/-}$ and *lcat*$^{-/-}$ mice compared to C57BL/6 mice (Fig. 4B, D, E).

3.4. Effects of Apoa1 and Lcat deficiency on plasma glucose homeostasis

To determine the effects of Apoa1- and Lcat-deficiency on plasma glucose homeostasis, *apoa1*$^{-/-}$ and *lcat*$^{-/-}$ mice were fed *ad libidum* western-type diet for 24 weeks and glucose tolerance test (GTT), insulin sensitivity test (IST) and pyruvate tolerance test (PTT) were performed at the beginning and at the end of the experiment (Fig. 5).

At week 0 of the experiment, *apoa1*$^{-/-}$ mice demonstrated a reduced glucose tolerance as indicated by the area under the curve (AUC) values in GTT compared to control mice (Fig. 5A, H). On the other hand, *lcat*$^{-/-}$ mice displayed increased hepatic gluconeogenesis as determined by the AUC values in PTT (Fig. 5C, J). No significant differences in insulin sensitivity among groups were detected when IST was performed (Fig. 5B, I). Moreover, all three mouse strains had normal fasting glucose levels (t = 0) between 60 and 80 mg/dl (Fig. 5A-C).

At week 24 of the experiment, glucose tolerance of *apoa1*$^{-/-}$ mice was significantly deteriorated (Fig. 5D, H). Similarly, these mice also displayed reduced insulin sensitivity compared to *lcat*$^{-/-}$ and C57BL/6 mice (Fig. 5E, I), indicating a normal response to intraperitoneally administered exogenous insulin when compared to week 0 (Fig. 5 I). Both *apoa1*$^{-/-}$ and C57BL/6 mice had similar levels of hepatic gluconeogenesis (Fig. 5F, J). Of note, feeding *lcat*$^{-/-}$ mice with western-

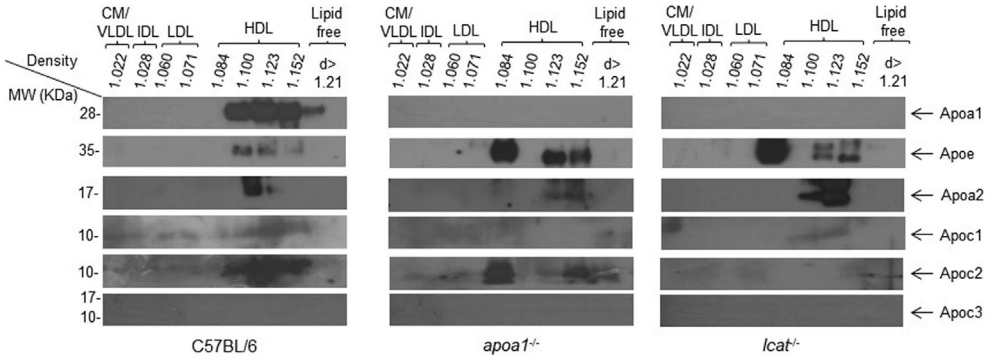

Fig. 2. Western blot analyses for plasma apolipoproteins. Lipoproteins were isolated by KBr density gradient ultracentrifugation from plasma samples of C57BL/6, *apoa1*$^{-/-}$ and *lcat*$^{-/-}$ mice after 24 weeks of feeding western-type diet ($n = 10$). Purified lipoprotein fractions were then analyzed by western blotting for Apoa1, Apoe, Apoa2, Apoc1, Apoc2 and Apoc3.

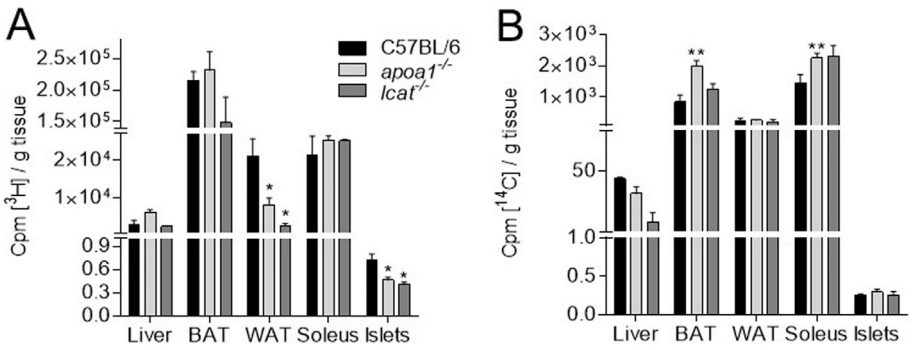

Fig. 3. Steady state levels of [^{3}H] and [^{14}C] tracers in tissues isolated from C57BL/6, *apoa1*$^{-/-}$ and *lcat*$^{-/-}$ mice, four hours following gavage administration of 200 μl extra virgin olive oil mixed with [^{3}H]-triolein and [^{14}C]-cholesterol. (A) [^{3}H] levels and (B) [^{14}C] levels measured in the indicated tissues for each mouse strain. Data were analyzed using Student's *t*-test and are presented as mean cpm of each tracer/g of each tissue ± S.E.M. ($n = 4$).

type diet for 24 weeks resulted in reduced hepatic gluconeogenesis compared to week 0 ($P < 0.01$) (Fig. 5J). *Apoa1*$^{-/-}$ mice also displayed higher fasting plasma glucose levels (126.4 ± 6.5 mg/dl, $P < 0.01$) compared to *lcat*$^{-/-}$ mice (100.9 ± 5.7 mg/dl) and C57BL/6 mice (91.1 ± 4.8 mg/dl) (Fig. 5D–F), which appear overall resistant to diet-induced glucose intolerance and insulin sensitivity.

3.5. Effects of Apoa1 and Lcat deficiency on skeletal muscle insulin sensitivity and HOMA index

Next, we performed an ISGU test in isolated intact soleus muscle from *apoa1*$^{-/-}$, *lcat*$^{-/-}$ and C57BL/6 mice at the beginning and end of the 24-week period, as described previously [36] and detailed in Materials and Methods.

Immediately prior to diet initiation (week 0) soleus muscles from C57BL/6 and *lcat*$^{-/-}$ mice showed considerable insulin sensitivity as indicated by the higher content of [^{3}H]-2-deoxy-D-glucose internalized upon insulin stimulation (0.83 ± 0.17 and 1.42 ± 0.04 pmol2-deoxyglucose/mg tissue/min, respectively, $P < 0.05$) (Fig. 6A). Similarly, insulin augmented hexose uptake in soleus muscles from *lcat*$^{-/-}$ mice in comparison to their basal level (0.52 ± 0.04 to 0.80 ± 0.04 pmol/2-deoxyglucose/mg tissue/min, $P < 0.05$). In contrast, muscles isolated from *apoa1*$^{-/-}$ mice appeared resistant to acute insulin stimulation (1.06 ± 0.16 and 1.18 ± 0.18 pmol/2-deoxyglucose/mg tissue/min, in the absence and presence of insulin respectively, $P > 0.05$).

Following feeding the western-type diet for 24 weeks, soleus muscles isolated from *apoa1*$^{-/-}$ mice remained resistant to insulin (1.36 ± 0.08 and 1.12 ± 0.08 pmol/2-deoxyglucose/mg tissue/min, in the absence and presence of insulin respectively, $P > 0.05$). In contrast, muscle isolated from C57BL/6 mice maintained their responsiveness to insulin (0.88 ± 0.07 and 1.19 ± 0.17 pmol/2-deoxyglucose/mg tissue/min, in the absence and presence of insulin, respectively). Similarly, the corresponding uptake levels in soleus muscles

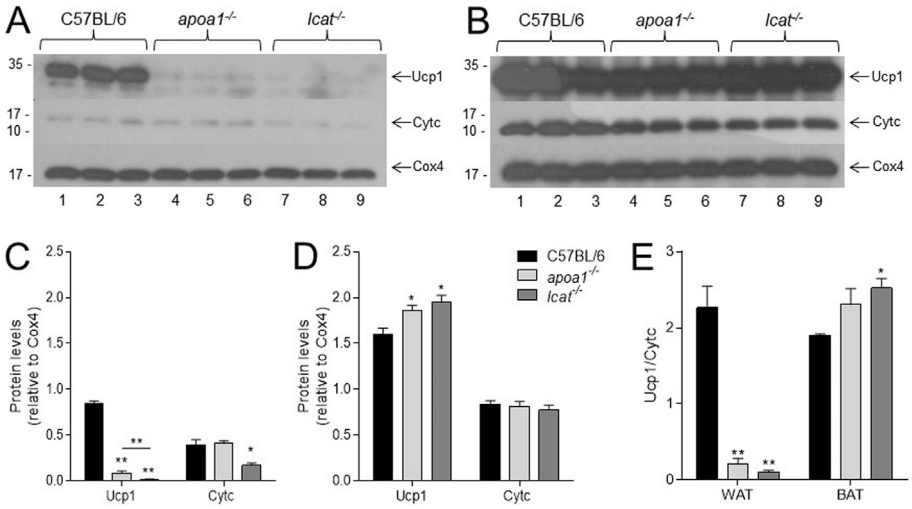

Fig. 4. Cytc and Ucp1 protein expression in isolated visceral WAT and BAT mitochondria from C57BL/6, *apoa1*$^{-/-}$ and *lcat*$^{-/-}$ mice fed western-type diet for 24 weeks. Representative western blot analyses (A, B) in pure mitochondrial extracts from visceral WAT (A) and BAT (B) isolated from C57BL/6, *apoa1*$^{-/-}$ and *lcat*$^{-/-}$ mice. Panels C, D show the semiquantitative measurement of mitochondrial Ucp1 and Cytc levels relative to mitochondrial Cox4 levels in WAT (C) and BAT (D) of C57BL/6, *apoa1*$^{-/-}$ and *lcat*$^{-/-}$ mice, based on the western of panels (A) and (B) respectively. Panel E indicates the Ucp1/Cytc ratio as an index of energy balance. Data were produced from the same blots probed with the indicated antibodies and analyzed using Student's *t*-test. Bars show the mean ± S.E.M ($n = 3$).

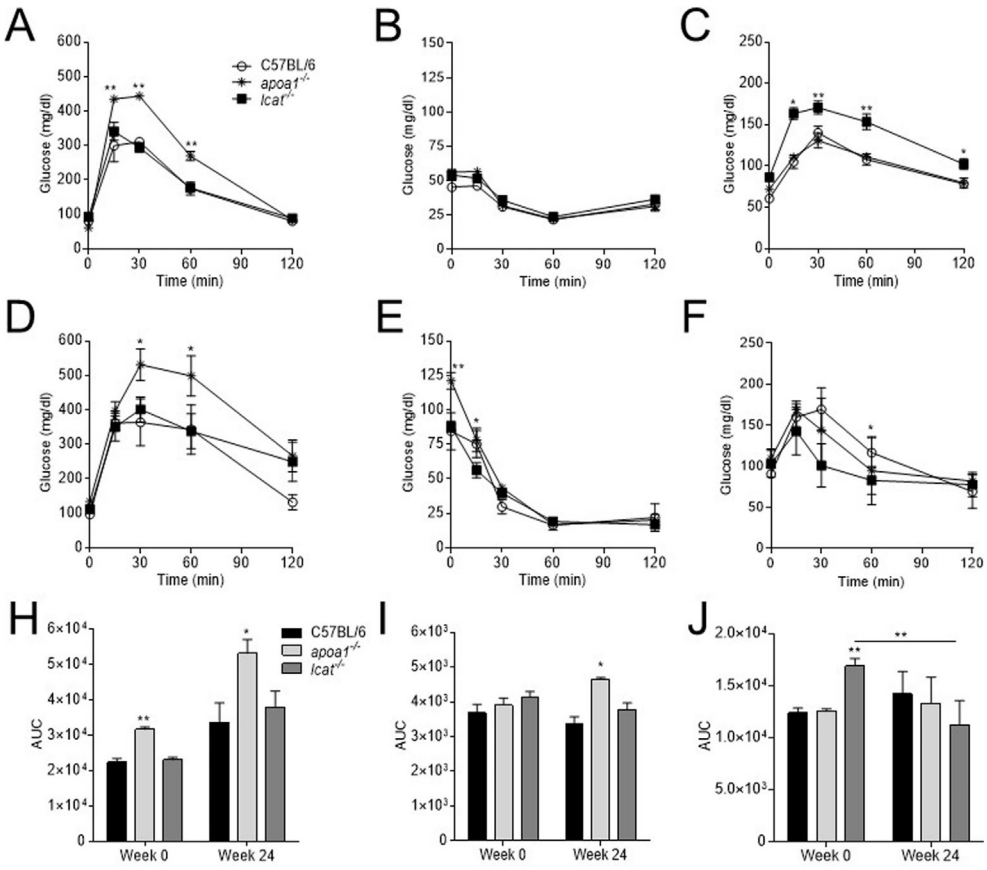

Fig. 5. Glucose tolerance test (GTT) (A, D, H), insulin sensitivity test (IST) (B, E, I) and pyruvate tolerance test (PTT) (C, F, J) at week 0 (A–C) and week 24 of the experiment (D-F). Panels H, I and J are graphic depictions of the area under the curve (AUC) of GTT (H), IST (I), and PTT (J). Data were analyzed using Student's *t*-test and are presented as mean ± S.E.M. (n = 4–9).

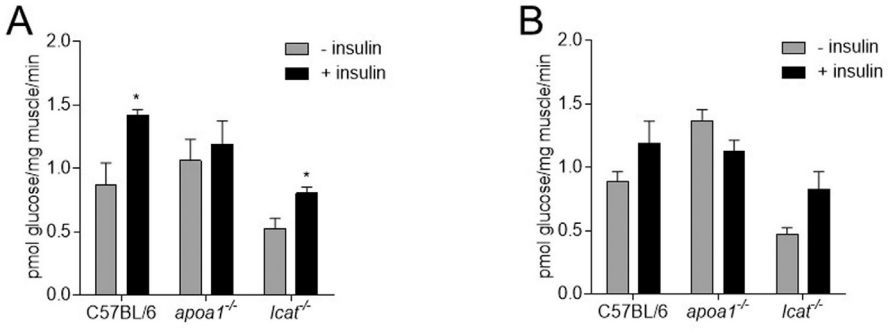

Fig. 6. Representative data of [^{3}H]-2-deoxy-D-glucose uptake by isolated soleus muscles from C57BL/6, *apoa1*$^{-/-}$ and *lcat*$^{-/-}$ mice at week 0 (A) and week 24 (B) of western-type diet feeding. Muscles were incubated in a solution containing [^{3}H]-2-deoxy-D-glucose in the presence (+insulin) or absence (−insulin) of actrapid insulin (500 nM). Panel (C) shows the fasting plasma glucose and insulin levels and calculated HOMA index of C57BL/6, *apoa1*$^{-/-}$ and *lcat*$^{-/-}$ mice at week 0 and week 24 of the experiment, respectively. Data in all panels were analyzed using Student's *t*-test and are presented as mean ± S.E.M. (n = 3–6).

C

		Glucose (mg/dl)	Insulin (mU/l)	HOMA index
Week 0	C57BL/6	81.1 ± 0.8	7.57 ± 0.07	**1.51** ± 0.01
	apoa1$^{-/-}$	60.9 ± 1.5	2.31 ± 0.01	**0.35** ± 0.01
	lcat$^{-/-}$	93.0 ± 1.0	12.93 ± 1.57	**2.97** ± 0.39
Week 24	C57BL/6	96.4 ± 1.9	19.37 ± 1.09	**4.61** ± 0.17
	apoa1$^{-/-}$	135.6 ± 2.1	18.83 ± 2.87	**6.29** ± 0.86
	lcat$^{-/-}$	112.1 ± 0.6	29.08 ± 1.47	**8.05** ± 0.37

from *lcat*$^{-/-}$ mice were 0.47 ± 0.04 and 0.82 ± 0.13 pmol/2-deoxyglucose/mg tissue/min, in the absence and presence of insulin respectively (Fig. 6B).

When fasting plasma insulin and glucose levels were measured, we found that all three mouse strains had elevated plasma glucose and insulin levels in response to feeding western-type diet for 24 weeks (Fig. 6C). Interestingly, all strains also had elevated HOMA index at the end of the 24-week period with *lcat*$^{-/-}$ mice showing the highest increase (Fig. 6).

3.6. Effects of Apoa1 and Lcat deficiency on insulin secretion

To further investigate the physiological mechanisms responsible for the differential effect of Apoa1- and Lcat-deficiency on diet-induced

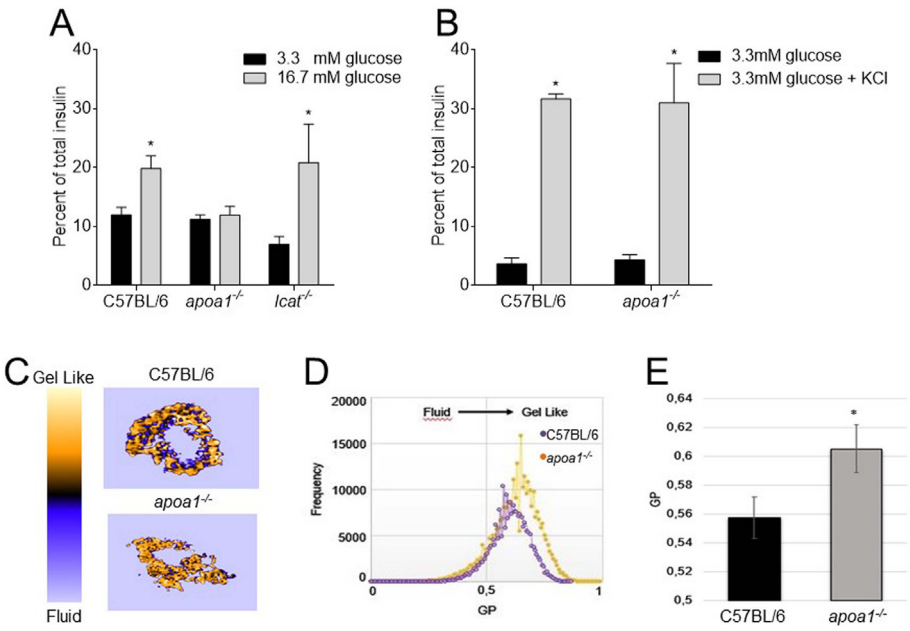

Fig. 7. Panels A and B show data of islets of Langerhans insulin secretion during GSIS. GSIS assay was performed, as described in Materials and Methods. Islets were successively incubated in Krebs-Ringer bicarbonate HEPES-BSA buffer containing 3.3 mM glucose, 16.7 mM glucose and finally in lysis buffer. Panel B shows data of *apoa1*$^{-/-}$ and C57BL/6 β-islets insulin secretion during GSIS performed with a solution containing 40 mM KCl. Islets were successively incubated in solutions containing 3.3 mM glucose, 3.3 mM glucose + KCl 40 mM and finally in lysis buffer. Data in all panels were analyzed using Student's *t*-test and are presented as mean percentage of total insulin content of cell lysates ± S.E.M. (n = 3–6). Panels C–E represent the analysis of membrane fluidity of β-cells isolated from C57BL/6 and *apoa1* −/− at the beginning of the experiment. (C) Representative images for cell membrane fluidity of C57BL/6 and *apoa1*$^{-/-}$ mice. (D) Generalized Polarization (GP) histogram and graph of GP values (E). Data in all panels were analyzed using Student's *t*-test and are presented as mean ± S.D. (n = 15–20).

glucose intolerance and insulin sensitivity, we performed a GSIS test on freshly isolated islets of Langerhans from *apoa1*$^{-/-}$, *lcat*$^{-/-}$ and C57BL/6 mice fed western-type diet for 24 weeks, as described previously [39] and detailed in Materials and Methods.

As shown in Fig. 7A, islets of Langerhans isolated from *lcat*$^{-/-}$ mice secreted less insulin in response to 3.3 mM glucose compared to those of *apoa1*$^{-/-}$ and control C57BL/6 mice (6.9 ± 1.3% for *lcat*$^{-/-}$ mice vs. 11.2 ± 0.7% for *apoa1*$^{-/-}$ mice vs. 11.9 ± 1.2% for C57BL/6 mice). When the islets were incubated with 16.7 mM glucose, those isolated from C57BL/6 and *lcat*$^{-/-}$ mice secreted more insulin upon stimulation (Fig. 7A). However, the stimulatory response to increased glucose levels was blunted in islets of *apoa1*$^{-/-}$ mice (Fig. 7A). In a separate experiment, depolarization of islets isolated from *apoa1*$^{-/-}$ and C57BL/6 mice with 40 mM KCl resulted in a comparable augmented secretion of insulin. This indicates that the islets of *apoa1*$^{-/-}$ mice maintain an intact secretory machinery that was not responsive glucose stimulation (Fig. 7B).

3.7. Effect of Apoa1 deficiency on cell membrane fluidity in isolated islets

Since changes in plasma membrane fluidity is known to affect the structure and responsiveness of ion-channels to natural stimuli [42], next we measured cell membrane fluidity in isolated islets of Langerhans from *apoa1*$^{-/-}$ and C57BL/6 mice. The measurement was performed by Laurdan two-photon microscopy, as described in Materials and Methods. We found that in islets from *apoa1*$^{-/-}$ mice cells had a more rigid membrane (i.e. less fluid) compared to islets from C57BL/6 mice. Fig. 7C shows representative fluidity images. The cumulative Generalized Polarization (GP) histogram in Fig. 7D shows a shift of *apoa1*$^{-/-}$ β-cells towards higher GP values, which correlates with a more gel-like (i.e., less fluid) state of plasma membrane. Fig. 7E depicts the average GP value increase of *apoa1*$^{-/-}$ vs C57BL/6 β-cells (0.605 ± 0.016 vs 0.557 ± 0.014, $P < 0.05$).

4. Discussion

Increasing amount of evidence suggests that in addition to its role in atheroprotection [1,3] HDL is also involved in the regulation of β-cell secretory function and peripheral tissue insulin sensitivity [27,32,43,44]. To better understand how changes in HDL metabolism may correlate with diet-induced obesity and T2DM we investigated the impact of Apoa1 and Lcat deficiency, two key proteins of peripheral HDL metabolic pathway, on these pathological conditions in mice. Deficiency in Apoa1 results in spherical HDL particles containing mainly esterified cholesterol and Apoe and Apoc2 and some Apoa2 [16] while deficiency in Lcat results in discoidal HDL particles containing primarily free cholesterol, Apoe and barely detectable levels of Apoa1 [45].

The present data show that *apoa1*$^{-/-}$ and *lcat*$^{-/-}$ mice became more sensitive to diet-induced obesity than control C57BL/6 mice, with *lcat*$^{-/-}$ animals becoming more obese than *apoa1*$^{-/-}$ animals (Fig. 1A). HDL from all three mouse strains presented distinct apolipoprotein composition (Fig. 2). HDL from C57BL/6 mice contained predominantly Apoa1, Apoa2 and Apoc2, and lower levels of Apoe. Even though feeding *lcat*$^{-/-}$ mice western-type diet resulted in an apparent lack of measurable plasma Apoa1, a finding consistent with previous observations [45], the apolipoprotein composition of the HDL in these mice is markedly different from the HDL of *apoa1*$^{-/-}$ mice. Specifically, *lcat*$^{-/-}$ mice had less Apoc2 and higher Apoa2 levels than *apoa1*$^{-/-}$ mice (Fig. 2).

These structural differences among HDL from the three mouse strains correlated with differences in peripheral postprandial plasma triglyceride and cholesterol tissue deposition (Fig. 3). Nevertheless, they could not account for the observed phenotypic differences in diet-induced obesity. Indeed, measurement of radioactive tracers following gavage administration of olive oil containing [^{3}H]-triolein and [^{14}C]-cholesterol showed a significantly lower dietary triglyceride tissue deposition in WAT of *apoa1*$^{-/-}$ and *lcat*$^{-/-}$ mice, although they accumulated significantly more visceral WAT than control C57BL/6 mice who were the same diet. Interestingly we also observed reduced [^{3}H]-tracer deposition in pancreatic β-islets isolated from *apoa1*$^{-/-}$ and *lcat*$^{-/-}$ mice (Fig. 3A). No difference in WAT [^{14}C]-tracer accumulation was apparent among groups indicating similar post-prandial cholesterol deposition. Nevertheless, *apoa1*$^{-/-}$ mice showed higher deposition of [^{14}C]-tracer in BAT and soleus muscle, suggesting increased dietary cholesterol uptake and storage in these tissues (Fig. 3B). The deposition of increased amounts of dietary cholesterol to soleus muscle may explain the development of insulin resistance of this tissue in response to feeding high fat diet, as previously reported [46].

Guided by these results and our previous experience with apolipoprotein E [34], we next hypothesized that Apoa1- or Lcat-deficiency may exert an effect on adipose tissue mitochondrial metabolic

activation [34]. When Cytc was analyzed as a marker of oxidative phosphorylation, WAT mitochondrial extracts of *apoa1*$^{-/-}$ and C57BL/6 animals displayed similar levels, indicating comparable oxidative phosphorylation activity in this tissue. However, *lcat*$^{-/-}$ mice expressed lower Cytc levels, suggesting that lack of functional Lcat had a selective negative impact on visceral WAT mitochondrial substrate oxidation towards energy production (heat and ATP). When Ucp1 was analyzed as a marker of non-shivering thermogenesis, WAT mitochondrial extracts, from C57BL/6 mice displayed considerable levels (Fig. 4A, C). However, similar analysis in *apoa1*$^{-/-}$ and *lcat*$^{-/-}$ mice displayed reduced Ucp1 levels, indicative of substantially reduced non-shivering thermogenesis in visceral WAT of these mice compared to the C57BL/6 group (Fig. 4A, C). Of note, Ucp1 levels were much lower in *lcat*$^{-/-}$ than *apoa1*$^{-/-}$ mice suggesting an even lower WAT oxidative phosphorylation capacity in the absence of Lcat. Similar analysis of BAT mitochondrial extracts revealed a rather small increase of Ucp1 levels in *apoa1*$^{-/-}$ and *lcat*$^{-/-}$ mice compared to C57BL/6 mice (Fig. 4B, D). No differences in BAT mitochondrial Cytc levels were found among the three mouse groups. These finding indicate that the increased sensitivity of *apoa1*$^{-/-}$ and *lcat*$^{-/-}$ mice towards diet-induced obesity is associated with reduced WAT mitochondrial non-shivering thermogenesis and that further suppression of WAT oxidative phosphorylation in *lcat*$^{-/-}$ mice renders them even more sensitive than *apoa1*$^{-/-}$ mice to weight-gain. Apparently, the small increase in BAT metabolic activity of *apoa1*$^{-/-}$ and *lcat*$^{-/-}$ mice may not suffice to counteract the massive decline in WAT mitochondrial metabolic activity of these mice when fed high-fat diet (Fig. 6A, C).

It is widely accepted that visceral obesity in subjects with metabolic syndrome predisposes to T2DM and other pathological components of the syndrome [25]. Contrasting this view, our findings show that only *apoa1*$^{-/-}$ mice developed glucose intolerance and insulin resistance following feeding high-fat diet (Fig. 5). This discovery supports the notion that obesity does not always induce glucose metabolic abnormalities. It is worth mentioning that *apoa1*$^{-/-}$ mice displayed reduced glucose tolerance even on normal chow diet, before they were challenged with the western-type diet (Fig. 5A). This observation shows that the lack of Apoa1 predisposes even lean animals fed chow-diet to disturbed glucose homeostasis, a pathology which is exacerbated by feeding a high-fat diet (Fig. 5D).

In agreement with these data, GSIS analysis in isolated pancreatic β-islets from *apoa1*$^{-/-}$ mice fed western-type diet for 24 weeks showed that insulin secretion in response to glucose stimulation is impaired in these mice compared to *lcat*$^{-/-}$ and C57BL/6 mice. Depolarization of cell membrane in islets of Langerhans from *apoa1*$^{-/-}$ mice following treatment with KCl resulted in significant amount of secreted insulin that was comparable to those of C57BL/6 mice (Fig. 7B) indicating that the secretory machinery in the islets of *apoa1*$^{-/-}$ mice remains intact and functional, but unresponsive to glucose (Fig. 7A). The deposition of dietary cholesterol and triglycerides to the islets of *apoa1*$^{-/-}$ mice (Fig. 3A, B) appears not to be a confounding factor to the impairment of their secretory function given that similarly levels of dietary lipids were also measured in the islets from *lcat*$^{-/-}$ mice.

It is well-established that changes in plasma membrane cholesterol content may impact cell membrane fluidity [47,48], which in turn may affect the structure and responsiveness of ion-channels to natural stimuli [42]. Since insulin secretion involves substrate stimulated and voltage-gated channels, we next determined how Apoa1-deficiency may influence cell membrane fluidity in isolated islets, using Laurdan staining and two-photon microscopy. This analysis revealed a significant shift of cell-membrane fluidity towards a more rigid gel-like structure, a physicochemical property that is associated with reduced stimulation of ion-channels [42]. Our data raise the possibility that in the more rigid membrane microenvironment of *apoa1*$^{-/-}$ mice, ATP-dependent potassium channels and/or voltage-gated Ca^{+2} channels become less responsive to their natural stimuli. In addition to impaired insulin secretion, *apoa1*$^{-/-}$ mice display insulin resistant skeletal muscles (Figs. 5E, I and 6B) which further exacerbates their systemic glucose tolerance as shown in GTT (Fig. 5D).

Conversely, islets of *lcat*$^{-/-}$ mice were more responsive to glucose stimulation than those of *apoa1*$^{-/-}$ mice (Fig. 7A). Moreover, hexose uptake by the skeletal muscles of *lcat*$^{-/-}$ mice remained responsive to insulin (Fig. 6) and *lcat*$^{-/-}$ mice maintained similar glucose tolerance and insulin sensitivity comparable to C57BL/6 mice (Fig. 5D, H, E, I), despite their massive increase in visceral WAT accumulation at week 24 of the diet.

When the HOMA index was determined, we found that all mouse strains had deteriorated insulin sensitivity in response to feeding high-fat diet, including *lcat*$^{-/-}$ and C57BL/6 mice. Interestingly, *lcat*$^{-/-}$ mice displayed the highest deterioration in insulin sensitivity based on their HOMA index, even though they displayed GTT and IST responses comparable to those of C57BL/6 mice. Apparently, when fed western-type diet for 24 weeks, *lcat*$^{-/-}$ mice enter a hyperinsulinemic state that overcomes their insulin resistance and maintains their plasma glucose levels physiological. In contrast, *apoa1*$^{-/-}$ mice have plasma insulin levels comparable to those of C57BL/6 mice but obviously their skeletal muscles fail to respond to insulin (Fig. 6B), while their islets remain unresponsive to glucose and unable to boost plasma insulin to a level that could overcome peripheral insulin resistance (Fig. 7A). Of course, in this interpretation it is very important to keep in mind the significant limitations of HOMA index use in mice. Even though HOMA index is a measure of insulin resistance widely used in numerous human clinical studies [38,49], the HOMA model has not been validated for use in rodents or any other animals and such use may violate the assumptions of the model [49].

Notably, the basal levels (−insulin) of glucose uptake by isolated soleus muscle in *lcat*$^{-/-}$ mice are significantly lower from the levels measured in the control C57BL/6 group, while stimulated levels (+insulin) reach those of the basal levels of the control group. These findings may indicate a shift from glucose metabolism to fatty acid oxidation and lower demand for glucose in *lcat*$^{-/-}$ mice. Yet, their soleus muscles remain highly sensitive to insulin stimulation at either week 0 or 24 (Fig. 6A, B, +insulin) indicating no induction of insulin resistance in the muscle of these animals following feeding the high fat diet.

5. Conclusions

Taken together, our data suggest that universal deletion of *apoa1* and *lcat* in mice fed western-type diet correlates with discreet effects on WAT metabolic activation and plasma glucose homeostasis. Apoa1-deficiency results in reduced WAT mitochondrial non-shivering thermogenesis. However, Lcat-deficiency causes a concerted reduction in both WAT oxidative phosphorylation and non-shivering thermogenesis, rendering *lcat*$^{-/-}$ mice the most sensitive in weight gain out of the three strains tested, followed by *apoa1*$^{-/-}$ mice. Nevertheless, only *apoa1*$^{-/-}$ mice show disturbed plasma glucose homeostasis due to non-responsive pancreatic β-islets to glucose and insulin resistant skeletal muscles. Our analyses show that both *apoa1*$^{-/-}$ and *lcat*$^{-/-}$ mice fed high-fat diet have no measurable Apoa1 levels in their plasma, suggesting that other HDL components may be responsible for the observed phenotypic differences of these groups. The precise role of Apoc2-HDL that is mainly present in *apoa1*$^{-/-}$ mice and Apoa2-HDL that is mainly present in the circulation of *lcat*$^{-/-}$ mice on WAT metabolic activation, pancreatic β-islet function and peripheral insulin resistance remain to be investigated.

Our data further indicate that changes in plasma apolipoprotein levels induced by hypolipidemic medications may impact WAT energy metabolism and glucose tolerance. It should be investigated if the weight gain and glucose intolerance associated with long term use of hypolipidemic medications, such as statins [50], is the result of altered plasma apolipoprotein levels triggered by these medications.

Transparency document

The Transparency document associated with this article can be found, in online version.

Author contributions

EX, GM, CC, EAK, EZ, performed experiments, analyzed data, participated in manuscript preparation and approved its final submitted form. KEK supervised the project, participated in the study design, performed experiments, analyzed data, prepared manuscript, approved its final submitted form and obtained funding for the study. SS and BD analyzed data, participated in manuscript preparation and approved its final submitted form.

Conflict of interest

The authors declare no conflict of interests/financial disclosure statement.

Funding

The authors of this article have collaborated in the framework of COST Action CM1201. Ms. E. Xepapadaki received funding for a short-term scientific mission (STSM) by the above COST action to visit the Hebrew University of Jerusalem, where she was trained on islet physiology in S. Sasson's laboratory (COST STSM Reference Number: COST-STSM-CM1201-16404). Ms. E. Xepapadaki and Dr. E. Karavia are currently supported by a graduate studentship (2017–2019) and a post-doctoral fellowship (2017–2019) respectively, funded by the Hellenic Scholarship Foundation (IKY). The work was supported by the project “INSPIRED - U OF PATRAS.” (MIS 5002550) of the Hellenic General Secreteriat for Research and Technology (GSRT), which is implemented under the Action “Reinforcement of the Research and Innovation Infrastructure”, funded by the Operational Programme "Competitiveness, Entrepreneurship and Innovation" (NSRF 2014-2020) and co-financed by Greece and the European Union (European Regional Development Fund).

References

[1] J.W. Gofman, F. Glazier, A. Tamplin, B. Strisower, L.O. De, Lipoproteins, coronary heart disease, and atherosclerosis, Physiol. Rev. 34 (1954) 589–607.
[2] T. Gordon, W.P. Castelli, M.C. Hjortland, W.B. Kannel, T.R. Dawber, High density lipoprotein as a protective factor against coronary heart disease. The Framingham study, Am. J. Med. 62 (1977) 707–714.
[3] R.J. Havel, H.A. Eder, J.H. BRAGDON, The distribution and chemical composition of ultracentrifugally separated lipoproteins in human serum, J. Clin. Invest. 34 (1955) 1345–1353.
[4] E.A. Karavia, E. Zvintzou, P.I. Petropoulou, E. Xepapadaki, C. Constantinou, K.E. Kypreos, HDL quality and functionality: what can proteins and genes predict? Expert. Rev. Cardiovasc. Ther. 12 (2014) 521–532.
[5] K.E. Kypreos, S. Gkizas, L.S. Rallidis, I. Karagiannides, HDL particle functionality as a primary pharmacological target for HDL-based therapies, Biochem. Pharmacol. 85 (2013) 1575–1578.
[6] G.J. Miller, N.E. Miller, Plasma-high-density-lipoprotein concentration and development of ischaemic heart-disease, Lancet 1 (1975) 16–19.
[7] E.M. Tsompanidi, M.S. Brinkmeier, E.H. Fotiadou, S.M. Giakoumi, K.E. Kypreos, HDL biogenesis and functions: role of HDL quality and quantity in atherosclerosis, Atherosclerosis 208 (2010) 3–9.
[8] V.I. Zannis, K.E. Kypreos, A. Chroni, D. Kardassis, E.E. Zanni, Lipoproteins and atherogenesis, in: J. Loscalzo (Ed.), Molecular Mechanisms of Atherosclerosis, Taylor & Francis, New York, NY, 2004, pp. 111–174.
[9] A. Chroni, T. Liu, I. Gorshkova, H.Y. Kan, Y. Uehara, A. von Eckardstein, V.I. Zannis, The central helices of apoA-I can promote ATP-binding cassette transporter A1 (ABCA1)-mediated lipid efflux. Amino acid residues 220-231 of the wild-type apoA-I are required for lipid efflux in vitro and high density lipoprotein formation in vivo, J. Biol. Chem. 278 (2003) 6719–6730.
[10] M.L. Fitzgerald, A.L. Morris, A. Chroni, A.J. Mendez, V.I. Zannis, M.W. Freeman, ABCA1 and amphipathic apolipoproteins form high-affinity molecular complexes required for cholesterol efflux, J. Lipid Res. 45 (2004) 287–294.
[11] I.C. Gelissen, M. Harris, K.A. Rye, C. Quinn, A.J. Brown, M. Kockx, S. Cartland, M. Packianathan, L. Kritharides, W. Jessup, ABCA1 and ABCG1 synergize to mediate cholesterol export to apoA-I, Arterioscler. Thromb. Vasc. Biol. 26 (2006) 534–540.
[12] M.A. Kennedy, G.C. Barrera, K. Nakamura, A. Baldan, P. Tarr, M.C. Fishbein, J. Frank, O.L. Francone, P.A. Edwards, ABCG1 has a critical role in mediating cholesterol efflux to HDL and preventing cellular lipid accumulation, Cell Metab. 1 (2005) 121–131.
[13] A.K. Soutar, C.W. Garner, H.N. Baker, J.T. Sparrow, R.L. Jackson, A.M. Gotto, L.C. Smith, Effect of the human plasma apolipoproteins and phosphatidylcholine acyl donor on the activity of lecithin: cholesterol acyltransferase, Biochemistry 14 (1975) 3057–3064.
[14] K.E. Kypreos, V.I. Zannis, Pathway of biogenesis of apolipoprotein E-containing HDL in vivo with the participation of ABCA1 and LCAT, Biochem. J. 403 (2007) 359–367.
[15] K.E. Kypreos, ABCA1 promotes the de novo biogenesis of apolipoprotein CIII-containing HDL particles in vivo and modulates the severity of apolipoprotein CIII-induced hypertriglyceridemia, Biochemistry 47 (2008) 10491–10502.
[16] S. Filou, M. Lhomme, E.A. Karavia, C. Kalogeropoulou, V. Theodoropoulos, E. Zvintzou, G.C. Sakellaropoulos, P.I. Petropoulou, C. Constantinou, A. Kontush, K.E. Kypreos, Distinct roles of apolipoproteins A1 and E in the modulation of high-density lipoprotein composition and function, Biochemistry 55 (2016) 3752–3762.
[17] E. Zvintzou, M. Lhomme, S. Chasapi, S. Filou, V. Theodoropoulos, E. Xapapadaki, A. Kontush, G. Spyroulias, C.C. Tellis, A.D. Tselepis, C. Constantinou, K.E. Kypreos, Pleiotropic effects of apolipoprotein C3 on HDL functionality and adipose tissue metabolic activity, J. Lipid Res. 58 (2017) 1869–1883.
[18] A.E. Kavo, L.S. Rallidis, G.C. Sakellaropoulos, S. Lehr, S. Hartwig, J. Eckel, P.I. Bozatzi, M. Anastasiou-Nana, P. Tsikrika, K.E. Kypreos, Qualitative characteristics of HDL in young patients of an acute myocardial infarction, Atherosclerosis 220 (2012) 257–264.
[19] E. Zvintzou, G. Skroubis, A. Chroni, P.I. Petropoulou, C. Gkolfinopoulou, G. Sakellaropoulos, D. Gantz, I. Mihou, F. Kalfarentzos, K.E. Kypreos, Effects of bariatric surgery on HDL structure and functionality: results from a prospective trial, J. Clin. Lipidol. 8 (2014) 408–417.
[20] Y.L. Marcel, P.K. Weech, T.D. Nguyen, R.W. Milne, W.J. McConathy, Apolipoproteins as the basis for heterogeneity in high-density lipoprotein2 and high-density lipoprotein3. Studies by isoelectric focusing on agarose films, Eur. J. Biochem. 143 (1984) 467–476.
[21] C.H. Saely, K. Geiger, H. Drexel, Brown versus white adipose tissue: a mini-review, Gerontology 58 (2012) 15–23.
[22] J. Heeren, H. Munzberg, Novel aspects of brown adipose tissue biology, Endocrinol. Metab. Clin. N. Am. 42 (2013) 89–107.
[23] T.J. Schulz, Y.H. Tseng, Brown adipose tissue: development, metabolism and beyond, Biochem. J. 453 (2013) 167–178.
[24] P. Flachs, M. Rossmeisl, O. Kuda, J. Kopecky, Stimulation of mitochondrial oxidative capacity in white fat independent of UCP1: a key to lean phenotype, Biochim. Biophys. Acta 1831 (2013) 986–1003.
[25] D.P. Schuster, Obesity and the development of type 2 diabetes: the effects of fatty tissue inflammation, Diabetes Metab. Syndr. Obes. 3 (2010) 253–262.
[26] Y. Sun, Y. Zhang, N. Li, H. Zhang, L. Zhou, L. Shao, Exposure to high levels of glucose increases the expression levels of genes involved in cholesterol biosynthesis in rat islets, Exp. Ther. Med. 8 (2014) 991–997.
[27] C. Morgantini, A. Natali, B. Boldrini, S. Imaizumi, M. Navab, A.M. Fogelman, E. Ferrannini, S.T. Reddy, Anti-inflammatory and antioxidant properties of HDLs are impaired in type 2 diabetes, Diabetes 60 (2011) 2617–2623.
[28] P.M. Okin, D.A. Hille, B.P. Wiik, S.E. Kjeldsen, L.H. Lindholm, B. Dahlof, R.B. Devereux, In-treatment HDL cholesterol levels and development of new diabetes mellitus in hypertensive patients: the LIFE study, Diabet. Med. 30 (2013) 1189–1197.
[29] P. Vollenweider, E.A. Von, C. Widmann, HDLs, diabetes, and metabolic syndrome, Handb. Exp. Pharmacol. 224 (2015) 405–421.
[30] N. Sakai, B.L. Vaisman, C.A. Koch, R.F. Hoyt Jr., S.M. Meyn, G.D. Talley, J.A. Paiz, H.B. Brewer Jr., S. Santamarina-Fojo, Targeted disruption of the mouse lecithin:cholesterol acyltransferase (LCAT) gene. Generation of a new animal model for human LCAT deficiency, J. Biol. Chem. 272 (1997) 7506–7510.
[31] E.A. Karavia, N.I. Papachristou, G.C. Sakellaropoulos, E. Xepapadaki, E. Papamichail, P.I. Petropoulou, E.P. Papakosta, C. Constantinou, I. Habeos, D.J. Papachristou, K.E. Kypreos, Scavenger receptor class B type I regulates plasma apolipoprotein E levels and dietary lipid deposition to the liver, Biochemistry 54 (2015) 5605–5616.
[32] E.A. Karavia, D.J. Papachristou, K. Liopeta, I.E. Triantaphyllidou, O. Dimitrakopoulos, K.E. Kypreos, Apolipoprotein A-I modulates processes associated with diet-induced nonalcoholic fatty liver disease in mice, Mol. Med. 18 (2012) 901–912.
[33] A.S. Augustus, Y. Kako, H. Yagyu, I.J. Goldberg, Routes of FA delivery to cardiac muscle: modulation of lipoprotein lipolysis alters uptake of TG-derived FA, Am. J. Physiol. Endocrinol. Metab. 284 (2003) E331–E339.
[34] A. Hatziri, C. Kalogeropoulou, E. Xepapadaki, E. Birli, E.A. Karavia, E. Papakosta, S. Filou, C. Constantinou, K.E. Kypreos, Site-specific effects of apolipoprotein E expression on diet-induced obesity and white adipose tissue metabolic activation, Biochim. Biophys. Acta 1864 (2018) 471–480.
[35] C. Constantinou, D. Mpatsoulis, A. Natsos, P.I. Petropoulou, E. Zvintzou, A.M. Traish, P.J. Voshol, I. Karagiannides, K.E. Kypreos, The low density lipoprotein receptor modulates the effects of hypogonadism on diet-induced obesity and related metabolic perturbations, J. Lipid Res. 55 (2014) 1434–1447.
[36] S. Sasson, E. Cerasi, Substrate regulation of the glucose transport system in rat skeletal muscle. Characterization and kinetic analysis in isolated soleus muscle and skeletal muscle cells in culture, J. Biol. Chem. 261 (1986) 16827–16833.

[37] Y.S. Lee, B.Y. Cha, K. Saito, H. Yamakawa, S.S. Choi, K. Yamaguchi, T. Yonezawa, T. Teruya, K. Nagai, J.T. Woo, Nobiletin improves hyperglycemia and insulin resistance in obese diabetic ob/ob mice, Biochem. Pharmacol. 79 (2010) 1674–1683.
[38] D.R. Matthews, J.P. Hosker, A.S. Rudenski, B.A. Naylor, D.F. Treacher, R.C. Turner, Homeostasis model assessment: insulin resistance and beta-cell function from fasting plasma glucose and insulin concentrations in man, Diabetologia 28 (1985) 412–419.
[39] G. Cohen, Y. Riahi, O. Shamni, M. Guichardant, C. Chatgilialoglu, C. Ferreri, N. Kaiser, S. Sasson, Role of lipid peroxidation and PPAR-delta in amplifying glucose-stimulated insulin secretion, Diabetes 60 (2011) 2830–2842.
[40] G. Maulucci, V. Labate, M. Mele, E. Panieri, G. Arcovito, T. Galeotti, H. Ostergaard, J.R. Winther, S.M. De, G. Pani, High-resolution imaging of redox signaling in live cells through an oxidation-sensitive yellow fluorescent protein, Sci. Signal. 1 (2008) l3.
[41] G. Maulucci, O. Cohen, B. Daniel, A. Sansone, P.I. Petropoulou, S. Filou, A. Spyridonidis, G. Pani, S.M. De, C. Chatgilialoglu, C. Ferreri, K.E. Kypreos, S. Sasson, Fatty acid-related modulations of membrane fluidity in cells: detection and implications, Free Radic. Res. 50 (2016) S40–S50.
[42] T.S. Tillman, M. Cascio, Effects of membrane lipids on ion channel structure and function, Cell Biochem. Biophys. 38 (2003) 161–190.
[43] C. Constantinou, E.A. Karavia, E. Xepapadaki, P.I. Petropoulou, E. Papakosta, M. Karavyraki, E. Zvintzou, V. Theodoropoulos, S. Filou, A. Hatziri, C. Kalogeropoulou, G. Panayiotakopoulos, K.E. Kypreos, Advances in high density lipoprotein physiology: surprises, overturns and promises, Am. J. Physiol. Endocrinol. Metab. 310 (2016) E1–E14.
[44] E.A. Karavia, D.J. Papachristou, I. Kotsikogianni, I.E. Triantafyllidou, K.E. Kypreos, Lecithin/cholesterol acyltransferase modulates diet-induced hepatic deposition of triglycerides in mice, J. Nutr. Biochem. 24 (2013) 567–577.
[45] P.I. Petropoulou, J.F. Berbee, V. Theodoropoulos, A. Hatziri, P. Stamou, E.A. Karavia, A. Spyridonidis, I. Karagiannides, K.E. Kypreos, Lack of LCAT reduces the LPS-neutralizing capacity of HDL and enhances LPS-induced inflammation in mice, Biochim. Biophys. Acta 1852 (2015) 2106–2115.
[46] A.L. Carey, A.L. Siebel, M. Reddy-Luthmoodoo, A.K. Natoli, W. D'Souza, P.J. Meikle, D. Sviridov, B.G. Drew, B.A. Kingwell, Skeletal muscle insulin resistance associated with cholesterol-induced activation of macrophages is prevented by high density lipoprotein, PLoS One 8 (2013) e56601.
[47] R.A. Cooper, Influence of increased membrane cholesterol on membrane fluidity and cell function in human red blood cells, J. Supramol. Struct. 8 (1978) 413–430.
[48] M.M. Gleason, M.S. Medow, T.N. Tulenko, Excess membrane cholesterol alters calcium movements, cytosolic calcium levels, and membrane fluidity in arterial smooth muscle cells, Circ. Res. 69 (1991) 216–227.
[49] T.M. Wallace, J.C. Levy, D.R. Matthews, Use and abuse of HOMA modeling, Diabetes Care 27 (2004) 1487–1495.
[50] D.I. Swerdlow, D. Preiss, K.B. Kuchenbaecker, M.V. Holmes, J.E. Engmann, T. Shah, R. Sofat, S. Stender, P.C. Johnson, R.A. Scott, M. Leusink, N. Verweij, S.J. Sharp, Y. Guo, C. Giambartolomei, C. Chung, A. Peasey, A. Amuzu, K. Li, J. Palmen, P. Howard, J.A. Cooper, F. Drenos, Y.R. Li, G. Lowe, J. Gallacher, M.C. Stewart, I. Tzoulaki, S.G. Buxbaum, A.D. van der, N.G. Forouhi, N.C. Onland-Moret, Y.T. van der Schouw, R.B. Schnabel, J.A. Hubacek, R. Kubinova, M. Baceviciene, A. Tamosiunas, A. Pajak, R. Topor-Madry, U. Stepaniak, S. Malyutina, D. Baldassarre, B. Sennblad, E. Tremoli, F.U. de, F. Veglia, I. Ford, J.W. Jukema, R.G. Westendorp, G.J. de Borst, P.A. de Jong, A. Algra, W. Spiering, A.H. Maitland-van der Zee, O.H. Klungel, B.A. De, P.A. Doevendans, C.B. Eaton, J.G. Robinson, D. Duggan, J. Kjekshus, J.R. Downs, A.M. Gotto, A.C. Keech, R. Marchioli, G. Tognoni, P.S. Sever, N.R. Poulter, D.D. Waters, T.R. Pedersen, P. Amarenco, H. Nakamura, J.J. McMurray, J.D. Lewsey, D.I. Chasman, P.M. Ridker, A.P. Maggioni, L. Tavazzi, K.K. Ray, S.R. Seshasai, J.E. Manson, J.F. Price, P.H. Whincup, R.W. Morris, D.A. Lawlor, G.D. Smith, Y. Ben-Shlomo, P.J. Schreiner, M. Fornage, D.S. Siscovick, M. Cushman, M. Kumari, N.J. Wareham, W.M. Verschuren, S. Redline, S.R. Patel, J.C. Whittaker, A. Hamsten, J.A. Delaney, C. Dale, T.R. Gaunt, A. Wong, D. Kuh, R. Hardy, S. Kathiresan, B.A. Castillo, P. van der Harst, E.J. Brunner, A. Tybjaerg-Hansen, M.G. Marmot, R.M. Krauss, M. Tsai, J. Coresh, R.C. Hoogeveen, B.M. Psaty, L.A. Lange, H. Hakonarson, F. Dudbridge, S.E. Humphries, P.J. Talmud, M. Kivimaki, N.J. Timpson, C. Langenberg, F.W. Asselbergs, M. Voevoda, M. Bobak, H. Pikhart, J.G. Wilson, A.P. Reiner, B.J. Keating, A.D. Hingorani, N. Sattar, HMG-coenzyme A reductase inhibition, type 2 diabetes, and bodyweight: evidence from genetic analysis and randomised trials, Lancet 385 (2015) 351–361.